Influence of Austempering Temperature on Microstructure and Mechanical Properties of High-Silicon Carbide-Free Bainitic Steel

Mattia Franceschi,* Luca Pezzato, Claudio Gennari, Denise Hanoz, Rachele Bertolini, Alberto Fabrizi, Marina Polyakova, Katya Brunelli, Franco Bonollo, and Manuele Dabalà

The microstructural evolution of a novel high-silicon carbide-free bainitic steel at different austempering temperatures is investigated. The microstructure is evaluated by means of optical and electron microscopy, X-ray diffraction, microhardness, and nanohardness. Results show a variation in the amount of stabilized retained austenite changing the temperature of the isothermal treatment. In particular, it is observed an increase in the retained austenite volume fraction increasing the temperature up to 350 °C, while further increase leads to a reduction. Moreover, increasing the isothermal holding temperature from 250 °C, through 300, 350, and 370 °C, a progressive bainite coarsening and an increase in the amount of stabilized carbon-enriched retained austenite are observed. Tensile tests reveal an excellent combination of mechanical properties: mechanical strength in the range 1276–1988 MPa and total elongation 0.18–0.44.

1. Introduction

Advanced high-strength steels (AHSS) are considered very attractive materials thanks to their outstanding strength combined with high ductility.[1–4] Several authors in the literature demonstrated their capability to achieve mechanical strength higher than 1.5 GPa with elongation above 15%.[5–8] This extremely favorable combination of mechanical properties makes these steel grades new leading actors in important industrial fields such as automotive (i.e., safe and lightweight components, which allow a strong reduction in oil consumption and CO_2 emission), railways application due to their high wear resistance in comparison with standard pearlitic steels,[2,9–12] and armor.[13]

Among the AHSS, carbide-free bainitic (CFB) steels are very attractive materials due to their multiphase microstructure consisting of supersaturated bainitic ferrite and carbon-enriched austenite.[14–17] The high amount of silicon (>2 wt%) allows the formation of CFB microstructure, with untempered martensite and high carbon retained austenite (with high stability). Silicon has the capability to suppress cementite precipitation and guarantee carbon partitioning in austenite increasing its stability to room temperature after final cooling during heat treatment.[18–22]

A crucial role in the behavior of these steels is played by the significant amount of retained austenite embedded in the microstructure.[5] Stable austenite at room temperature gives a strong contribution to the mechanical properties of these alloys thanks to its transformation into martensite when subjected to mechanical stress (transformation-induced plasticity [TRIP] effect).[15] It can be found in two morphologies which have different properties: 1) film-like retained austenite; 2) retained austenite in form of blocks.[5,10,22–25] Film-like austenite is embedded between bainitic ferrite plates and its thickness is in the order of nanometers and its carbon content is higher compared to blocky austenite. Thanks to the high carbon content, filmy austenite shows high stability against stress application, low tendency to the transformation, allows toughness improvement, and represents an obstacle to crack propagation. Instead, blocky-type austenite is less carbon enriched and characterized by inhomogeneous

M. Franceschi, L. Pezzato, C. Gennari, D. Hanoz, K. Brunelli, M. Dabalà
Department of Industrial Engineering
University of Padova
Via Marzolo 9, 35131 Padova, Italy
E-mail: mattia.franceschi@phd.unipd.it

R. Bertolini
Department of Industrial Engineering
University of Padova
Via Venezia 9, 35131 Padova, Italy

A. Fabrizi, F. Bonollo
Department of Management and Engineering
University of Padova
Stradella San Nicola 3, 36100 Vicenza, Italy

M. Polyakova
Department of Mechanical Engineering and Metallurgical Technologies
Nosov Magnitogorsk State Technical University
pr. Lenina, 38, 455000 Magnitogorsk, Russia

ADVANCED
SCIENCE NEWS
www.advancedsciencenews.com

steel
research
international
www.steel-research.de

composition and it was found that blocks can transform at low strain, as demonstrated by several authors.[23]

The presence of untempered martensite is linked to the limitation of the bainitic transformation, whose extension is determined by the T_0 curves. It represents the locus of points at which ferrite and austenite have the same Gibbs free energy and the maximum carbon in austenite, above which displacive transformation is hindered.[9,14,26,27]

In the literature, several studies were carried out to elucidate the effect of heat treatment parameters, during austempering, in order to optimize the microstructure and maximize the mechanical response of such steel grades, in particular in high-carbon steels. Many works were dedicated to the investigation of austenitizing conditions,[28–30] while many authors investigated the effect of different conditions for the isothermal treatments.[7,31–34]

According to Son et al.,[7] an increase in the austempering temperature leads to thicker bainitic ferrite plates due to the lower austenite strength that allows coarser subunit plates. Furthermore, in total agreement with Kumar et al.,[31] an increase in the untransformed austenite volume fraction, in high-silicon austempered spring steel, occurs when the isothermal transformation temperature is increased. According to Palaksha et al.,[32] this phenomenon is correlated to an increase in the carbon diffusion rate, which occurs at progressively higher austempering temperatures. Moreover, isothermal treatments at higher temperatures favor the presence of large austenitic blocks,[33] due to the lower chemical driving force associated with the bainitic transformation.

Concerning the influence of different holding times during the isothermal step of the austempering treatment, Liu et al.[34] demonstrated that longer austempering times decrease the amount of blocky austenite and increase the stability of stable carbon-enriched retained austenite because this leads to the formation of larger volume fraction of bainitic ferrite that increases with time.

The tensile properties of CFB steels were presented by several authors, including,[8,30,35–38] reaching an exceptional combination of tensile strength and ductility. Caballero et al.[6] obtained ultimate tensile strength (UTS) higher than 2 GPa and with low-temperature austempering, in the range 220–250 °C for 16 and 22 h, in order to complete the bainitic transformation.

Nowadays industry requires new materials, characterized by high mechanical performances in order to reduce the weight of the parts to reduce fuel consumption, with the aim of reducing the environmental impact which is a question of primary importance. Moreover, the requirement regards also the cost of the materials themselves; therefore, a deep study is necessary to produce new alloys without the addition of expensive alloying elements, such as Cr, V, and Mo. In addition, most of the work in the literature concerns high-carbon steels[21,23,39,40] that have limited weldability, reducing their applicability.

Thus, this article aims to characterize a novel composition of a medium-carbon high-silicon CFB steel, with Si weight fraction higher than 3%. In particular, a study of the effect of the isothermal treatment on the microstructure and on the mechanical properties has been carried out.

2. Experimental Section

2.1. Material Production

The chemical composition of the investigated steel measured with optical emission spectroscopy (OES) is shown in **Table 1**. A 40 kg ingot (40 × 18 × 8.5 cm) was produced with a vacuum induction furnace, by high purity raw material. The ingot was then hot rolled to a 20 mm-thick sheet at 1200 °C in seven passes. Detailed information, including pass temperature, thickness reduction, and applied force, about the rolling process is reported in **Table 2**.

2.2. Heat Treatments

The design of heat treatments was performed with the support of JmatPro software. Continuous colling transformation (CCT) and time–temperature transformation (TTT) curves are presented in **Figure 1**. A_3 and M_s were estimated equal to 843 and 238 °C, respectively. The M_s value is in good agreement with that estimated, equal to 228 °C, utilizing empirical formula proposed by Steven–Haynes.[41]

Heat treatment setup for the thermal cycles consisted of a Carbolite tubular electrical furnace for prenormalization treatment and the reaustenitization of the austempering treatment. A Naberterm 3000 electric muffle furnace was employed for the austempering step of the treatment for bainitic transformation. The temperature of the samples (30 × 15 × 5 mm) was constantly measured by a spot-welded K-thermocouple during the entire thermal cycle on the specimen surface. A forced air-cooling system for the intermediate cooling phase of the treatment was used, while the final cooling to room temperature was performed in water. The scheduled treatments were as follows: 1) prenormalization: austenitization at 900 °C with a heating rate of 5 °C s^{-1}, dwell time of 30 min, and cooling in calm air outside the furnace at 10 °C s^{-1} (**Figure 2**); 2) austempering: austenitization at 900, 5 °C s^{-1} heating rate, and holding time of 30 min. Cooling step in forced air at 10 °C s^{-1} until it reach the temperature for austempering treatment (250, 300, 350, and 370 °C) and held for 2 h (Figure 2). At the end of the treatment, specimens were cooled in water at 40 °C s^{-1}.

2.3. Microstructural Characterization

The microstructure of the samples was investigated through optical light microscopy (OM, Leica DMRE, Leica Microsystems,

Table 1. Chemical composition of investigated alloys (wt%).

Fe	C	Si	Mn	Al	Cr	Ni	Mo	Cu	Ti	V	P	S
Bal.	0.38	3.2	2.65	0.1	0.05	0.05	0.02	0.05	0.0011	0.0056	0.008	0.007

**ADVANCED
SCIENCE NEWS**

www.advancedsciencenews.com

**steel
research**
international

www.steel-research.de

Table 2. Description of hot rolling steps.

No. of passes	Temperature [°C]	Thickness reduction [%]	Force [ton]
1	1200	2	5.4
2	1148	29.7	53.3
3	1095	21.9	49.4
4	1081	22.0	55.8
5	1073	22.1	68.0
6	1065	21.9	65.8
7	1051	22.2	80.7

S.r.l., Milan, Italy) and scanning electron microscopy (SEM) with a Leica Cambridge Leo Stereoscan 440 (Leica Microsystems S.r.l., Milan, Italy). The samples were prepared according to the standard metallographic preparation, by cutting with SiC disks, with an oil–water emulsion for lubrication, and then were hot mounted in phenolic resin. The samples were then ground with 320, 500, 800, and 1200 grit water-lubricated SiC papers and then polished with polycrystalline diamond pastes 6, 3, and 1 μm. An etching with Nital 5 (95 mL ethanol with 5 mL Nitric acid) was performed. The evaluation of bainitic ferrite and filmy retained austenite thickness was performed on at least five micrographs taken at high magnification (15 000×), through the linear intercept method, in the direction perpendicular to the sheaf length, with ImageJ software and applying the stereological correction $L = 2/\pi$.[42]

X-ray diffraction (XRD) analysis was performed on the specimens with a Siemens D500 X-ray diffractometer (Siemens, Munich, Germany), equipped with a monochromator placed on the detector side and a Cu Kα radiation tube, working at 40 kV and 30 mA. An angular range $2\theta = 40°–105°$ was investigated, fixing a step scan of 0.025° and a counting time of 3 s. Pattern analysis and phase quantification were performed through the Rietveld method with the support of MAUD software.[43]
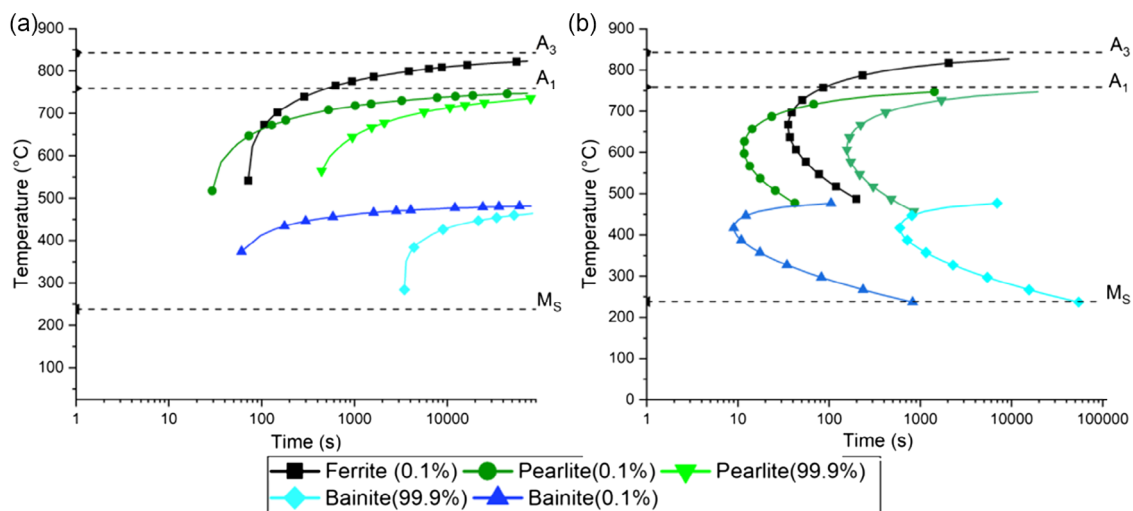
Electron backscattered diffraction (EBSD) was employed for additional crystallographic investigation with an FEI QUANTA
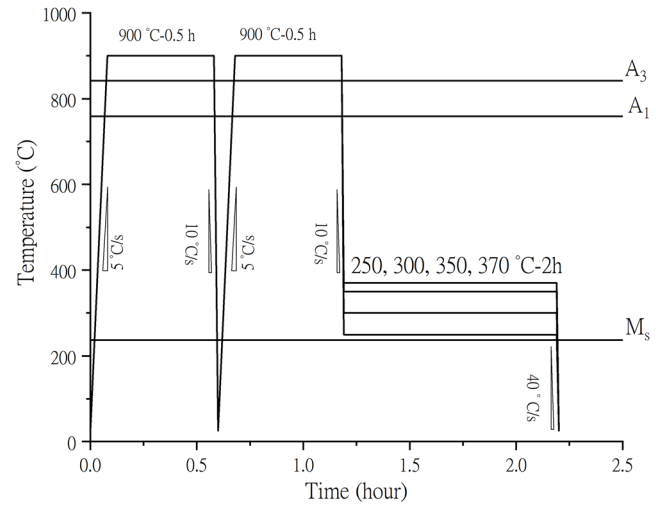
Figure 2. Heat treatment scheme.

250 FEG-SEM (Thermo Fisher Scientific, Hillsboro, OR, USA) operating at 20 kV, with the support of an AMETEK EBSD (AMETEK BV, Tilburg, The Netherlands) system and OIM Analysis software. Samples for EBSD were mounted with conductive resin and after standard preparation, a final polishing with silica suspension (200 and 40 nm) was performed. The investigated area was approximately $200 \times 200\ \mu m^2$, the step scan was fixed to 50 nm, and the confidence index was 0.1.

Transmission electron microscopy (TEM) was also used for microstructural characterization and phase identification by selected area diffraction (SAED), with a JEOL JEM 200CX (Jeol Ltd., Tokyo, Japan) operating at 160 kV. Specimen preparation included first cutting 150 μm thin foils, with an ATM 210A microcutting machine (Verder Scientific S.r.l., Italy) and mechanical ground down to a thickness of less than 50 μm. After that, 3 mm disks were obtained by mechanical punching and twin-jet electropolished up to perforation with a STRUERS TENUPOL-3 (Struers S.A.S., Milan, Italy)

Figure 1. a) CCT and b) TTT (curves).

ADVANCED
SCIENCE NEWS

www.advancedsciencenews.com

steel research
international

www.steel-research.de

using a 95% acetic acid (CH_3COOH) and 5% perchloric acid ($HClO_4$) solution, at 18 V and room temperature. Electron diffraction patterns were indexed according to ref. [44].

2.4. Tensile Tests

Tensile test specimens were machined from the base material to obtain dog-bone samples with a gauge length of 32, 6.25 mm width, and 6 mm in thickness, in agreement with ASTM A370-20. The tests were performed on a Galdabini (Galdabini Cesare s.r.l., Varese, Italy) tensile test machine with a 600 kN maximum force. Elongation was measured considering the crosshead displacement, and the force by the load cell. Three specimens were prepared for each condition and the average value is presented. The applied strain rate was equal to $10^{-3}\,s^{-1}$. Tensile tests were carried out at room temperature.

2.5. Hardness Tests

Vickers microhardness measurements were conducted on a Leitz DURIMET hardness tester, with a load of 300 g. Five indentations were performed on each specimen and results will be presented in form of mean value plus standard deviation.

Nanoindentation measurements were carried out using an iMicro from Nanomechanics Inc. nanoindenter to evaluate the hardness and elastic modulus of the material. Indentation maps consisted of a square of $200 \times 200\,\mu m^2$ area on which 25 indentations were performed using a load of 200 mN on three different zones across the sections of each sample. Indentations were spaced sufficiently far apart so that the indentation behavior was not affected by the presence of adjacent indentations, in accordance with the ISO standard 14577-4:2016. The procedure included the sample positioning under the tip, approach to the surface, loading, unloading, and retraction. From the load and
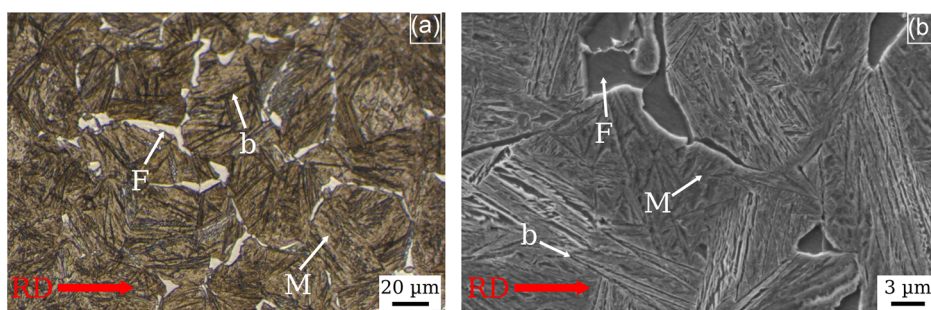
Figure 3. a) OM and b) SEM micrograph (SE mode) of the investigated alloy along the RD in as-received-state (F, ferrite; M, martensite; and b, bainite).
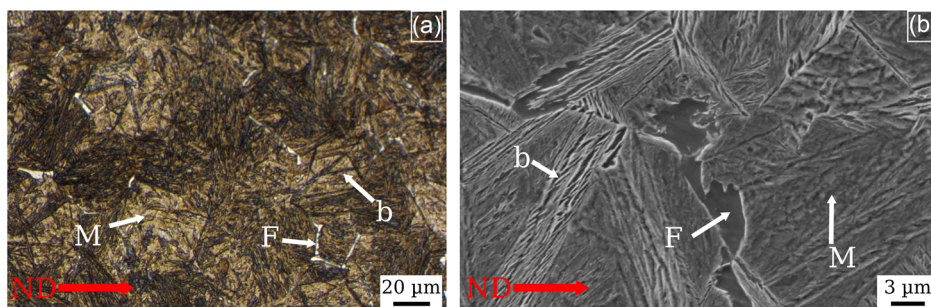
Figure 4. a) OM and b) SEM (SE mode) of the investigated alloy along the ND (ND in as-received state) (F, ferrite; M, martensite; and b, bainite).
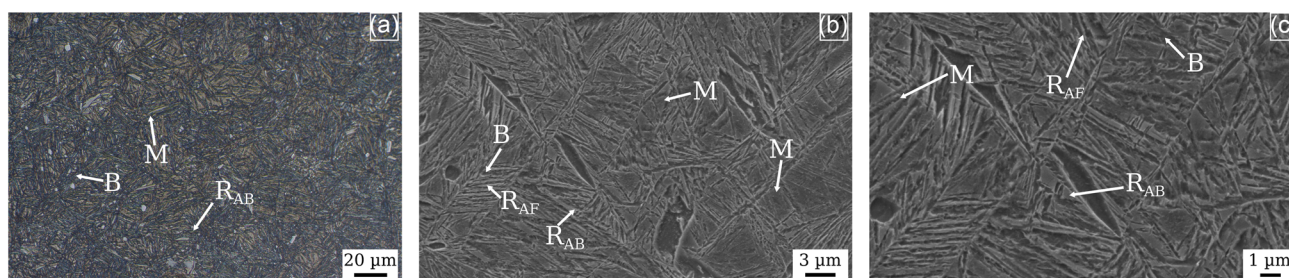
Figure 5. a) OM and b,c) SEM micrographs (SE mode) of the investigated alloy after austempering treatment at 250 °C for 2 h (M, martensite; B, bainitic ferrite; R_{AB}, retained austenite blocks; R_{AF}, retained austenite films).

ADVANCED
SCIENCE NEWS

www.advancedsciencenews.com

steel
research
international

www.steel-research.de

depth data at each test location, the contact stiffness, hardness, and modulus can be calculated using the standard Oliver and Pharr method. A diamond Berkovich tip was used for all the tests.

3. Results and Discussion

3.1. Microstructure

The microstructure of the as-received material along the rolling direction (RD) is depicted in the optical and electron scanning micrograph in **Figure 3**a,b. The microstructure consists of a mixture of martensite (M), bainitic ferrite sheaves (b), and proeutectoid ferrite (F) located at the grain boundaries.[45] A similar microstructure is shown in the OM and SEM micrographs taken in the normal rolling direction (ND) (**Figure 4**a,b). No preferential grain orientation with equiaxed grains is found along the RD.

From the examination of the microstructure by optical and electron microscopy of the samples treated at 250 °C, displayed
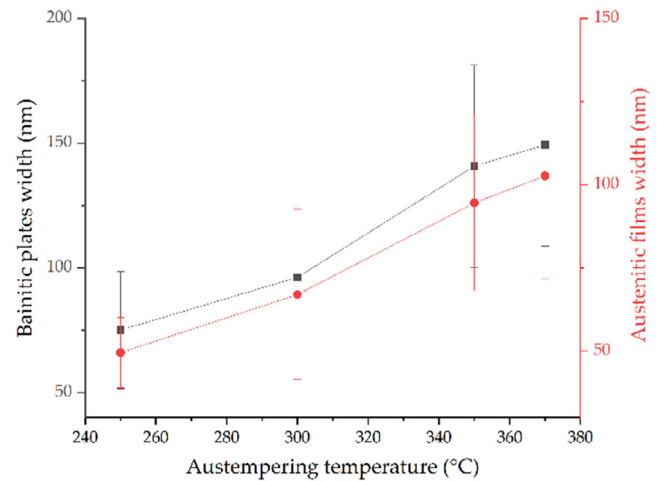

Figure 9. Variation of bainitic plates and film of retained austenite thickness with austempering temperature.
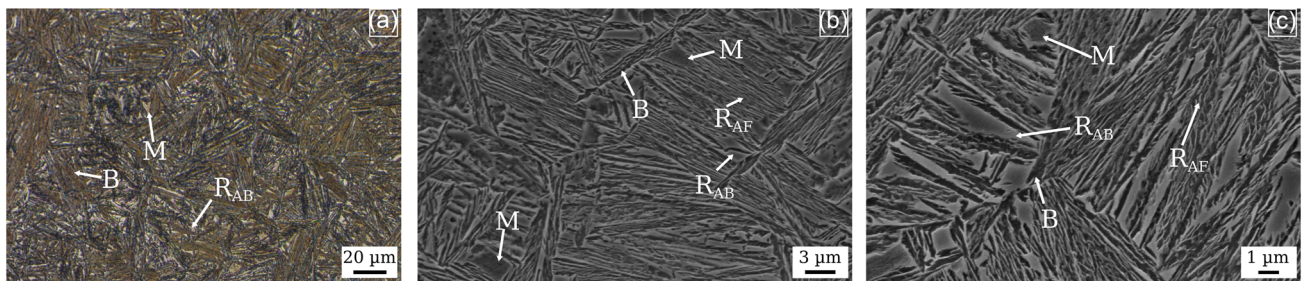
Figure 6. a) OM and b,c) SEM micrographs (SE mode) of the investigated alloy after austempering treatment at 300 °C for 2 h (M, martensite; B, bainitic ferrite; R_{AB}, retained austenite blocks; R_{AF}, retained austenite films).
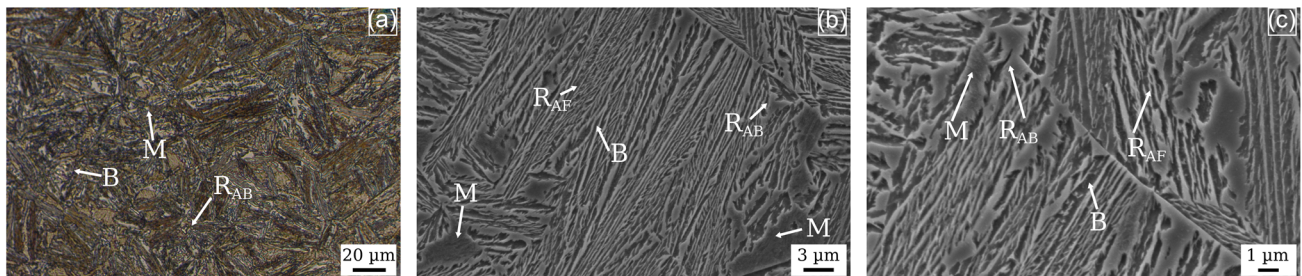
Figure 7. a) OM and b,c) SEM micrographs (SE mode) of the investigated alloy after austempering treatment at 350 °C for 2 h (M: martensite, B: bainitic ferrite, R_{AB}: retained austenite blocks, R_{AF}: retained austenite films).
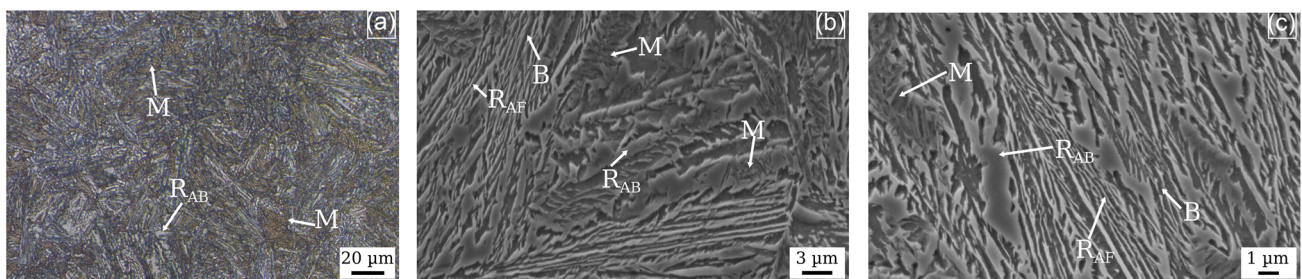
Figure 8. a) OM and b,c) SEM micrograph (SE mode) of the investigated alloy after austempering treatment at 370 °C for 2 h (M, martensite; B, bainitic ferrite; R_{AB}, retained austenite blocks; R_{AF}, retained austenite films).

ADVANCED
SCIENCE NEWS

www.advancedsciencenews.com

steel
research
international

www.steel-research.de

in **Figure 5**, it is possible to observe the typical CFB microstructure morphology, consisting of a mixture of bainitic ferrite, films of carbon-enriched retained austenite, and austenite blocks.

In **Figure 6**, **7**, and **8**, optical (a) and SEM (b, c) micrographs of the specimen austempered for 2 h at 300, 350, and 370 °C are depicted, while the measurements on bainitic plates are depicted in **Figure 9**. A prevalent CFB microstructure was obtained, in agreement with several works present in the literature on similar steels.[6,46–48] It is possible to recognize filmy retained austenite (R_{AF}) sandwiched between bainitic ferrite plates in the sheaves (B). While in correspondence with the prior austenite grain boundaries and different sheaves, martensitic islands (M) and blocks of retained austenite were also individuated (R_{AB}). In this case, it is possible to observe that there is an appreciable increase in the bainitic ferrite and austenite thickness.[7,35] The increase in the bainitic ferrite plate thickness is strictly related to the austenite yield strength (YS), as reported by Bhadeshia:[27] at higher temperatures austenite YS is lower and plate growth can be easily accommodated. Moreover, owing to the faster dynamic recovery, that takes place at high temperatures, weakens austenite, and leads to the formation of coarser plates.[27]

The presence of martensite in the investigated samples may be acribed to two factors: on the one hand, even though the simulated CCT curve indicates the that the bainitic transformation reaches completion, it may fail in predicting the appropriate sufficient isothermal holding time;[49] on the other hand, even though the transformation temperature reaches completion, it may guarantee enough carbon enrichment to lower the untransformed retained austenite martensite start below room temperature, which is more probable at high transformation temperature. Part of retained austenite, which did not decompose into bainite and which is not sufficiently carbon enriched, during final cooling to room temperature undergoes a martensitic transformation.

### 3.2. Electron Back-Scattered Diffraction

Complete microstructural characterization has been performed by means of EBSD on selected samples, in order to investigate the distribution, shape, and size of retained austenite in the different austempered specimens. No preferential orientation of grains was observed, suggesting that the pretreatment is efficacious in removing the effects deriving from the previous thermomechanical process (**Figure 10**a). In addition, the random orientation of the sheaves suggests the multiplicity of the variants observed in the orientation map because the bainitic transformation is isotropic.[50] In fact, as proposed by the authors[3] and Eres-Castellanos and co-authors, the transformation in the absence of external stress is isotropic and there is no favored growth of bainitic ferrite subunits.

From Figure 10b it is possible to understand the distribution of retained austenite, colored in green, in the CFB matrix (red). The phase map reveals the presence of small films of austenite with nanometric thickness between bainitic ferrite plates and austenitic blocks with a round shape located at the grain boundaries.

3.3. TEM

TEM allowed further detailed microstructural investigation (**Figure 11** and **12**) of carbide-free bainite in the investigated alloys. As shown before, the microstructure consists of bainitic ferrite and films of retained austenite sandwiched between
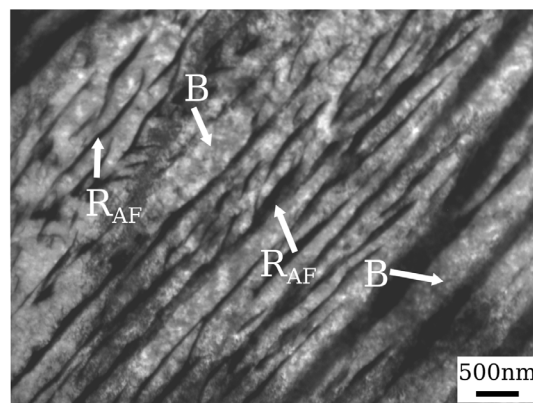
Figure 11. TEM bright field micrographs of the specimen treated at 300 °C for 2 h.
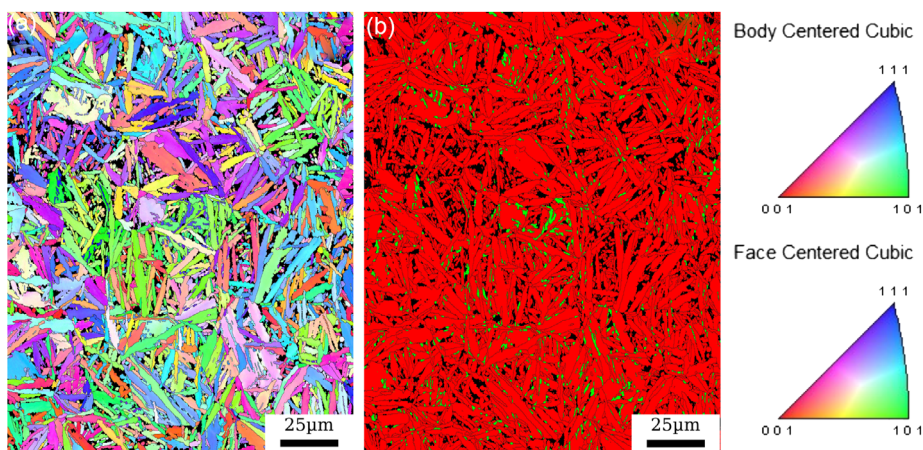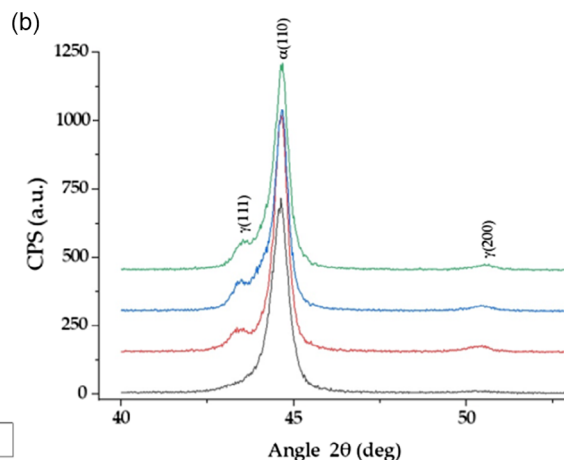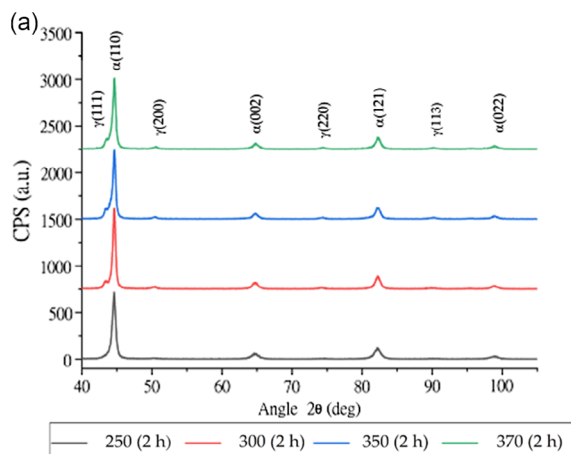

Figure 10. a) Grain orientation map and b) phase identification for the specimen subjected to austempering at 350 °C.
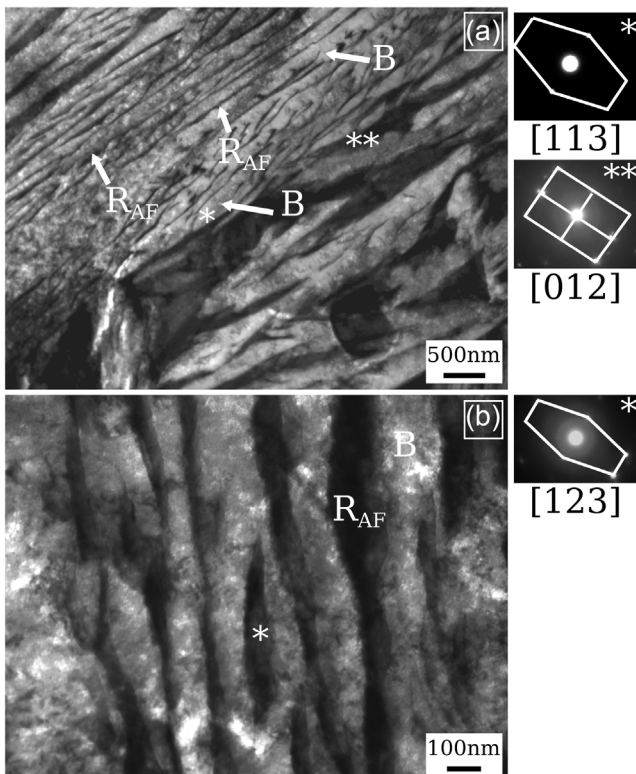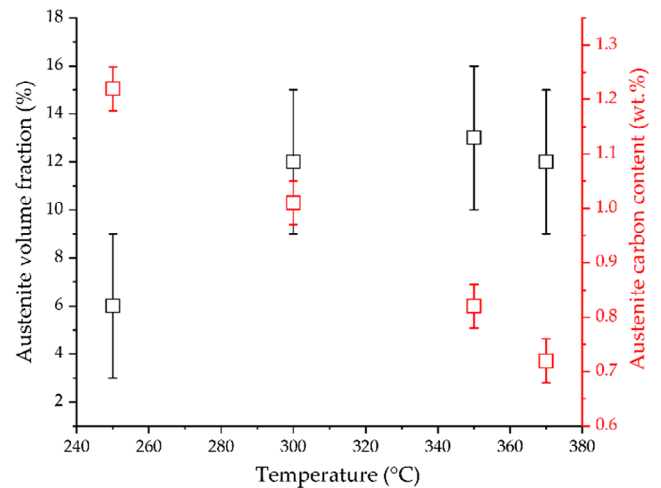
Figure 12. a,b) TEM bright field micrographs of the specimen treated at 350 °C for 2 h (B_F, bainitic ferrite; R_{AF}, retained austenite films). In a) * indicates the SAED pattern of bainitic ferrite, ** indicates the SAED pattern of austenite; in b) * refers to austenite SAED pattern.

Figure 14. Variation of retained austenite volume fraction and carbon content with the austempering temperature for 2 h holding time (before the tensile tests).

ferritic plates, both in nanoscale, validating the previous assumptions, in agreement with refs. [14,51,52]. Furthermore, TEM images show the presence of tangles of dislocations within the bainitic ferrite plates.

For all the observed specimens, TEM failed to detect cementite both within bainitic ferrite subunits or sandwiched between the plates, confirming the effective ability of silicon and aluminum to suppress cementite precipitation.

3.4. XRD

Figure 13 shows the XRD patterns of the samples austempered at 250, 300, 350, and 370 °C for 2 h, with an inset focusing on the main two reflections, while results of the Rietveld refinement on the XRD acquired patterns (amount of stabilized retained austenite V_γ) are shown in Table 2. The amount of stabilized retained austenite in the alloy increases with the austempering temperature (from 250 to 350 °C), in agreement with the literature,[7,32] thanks to the faster carbon diffusion promoted by the higher temperature. At higher temperatures (370 °C), a decrease in retained austenite is observed, in agreement with ref. [53].

Figure 14 and Table 2 show also the results of the carbon content calculation in the retained austenite (x_γ) and bainitic ferrite/martensite. Carbon content decreases increasing the austempering temperature, in agreement with Putatunda et al.[53] and with the trend of T_0 curves with temperature.[14] Moreover, the evaluation of the carbon content was performed also for the mixture of bainitic ferrite and martensite and because

Figure 13. a) XRD patterns before tensile tests; b) zoom of the main austenite–ferrite peaks.

the technique is blind in distinguishing the two tetragonal phases and an average value is reported. It can be seen that bainitic ferrite mixture is characterized by carbon supersaturation, in agreement with Caballero et al.[54]

3.5. Tensile Tests and Characterization after Mechanical Tests

In order to shed light on the effect of the isothermal holding temperature, and the microstructural constituents on the mechanical properties in this medium-carbon, high-silicon steel, the mechanical behavior tensile tests were performed on the various samples. The engineering stress–strain curves and tensile properties are displayed in **Figure 15**, **16** and **Table 3**. The best performances both in terms of YS and UTS (1638 and 1988 MPa, respectively) were obtained for isothermal holding at 250 °C. Then the greater the holding temperature, the lower both YS and UTS, in agreement with refs. [23,32]. A different trend is followed for the fracture strains: first, increasing the austempering temperature from 250 to 300 °C, an increase in ductility and total elongation is observed, but for higher holding temperature strong reduction occurred. Nevertheless, all the samples showed an excellent strength-to-elongation ratio. Concerning the behavior of the specimens treated at 350 and 370 °C, it is possible to observe limited plastic deformation and necking with respect to the previous samples (Table 3), even if it was characterized by a significant amount of retained austenite (13% and 12%, respectively), similar to sample treated at 300 °C. This phenomenon and
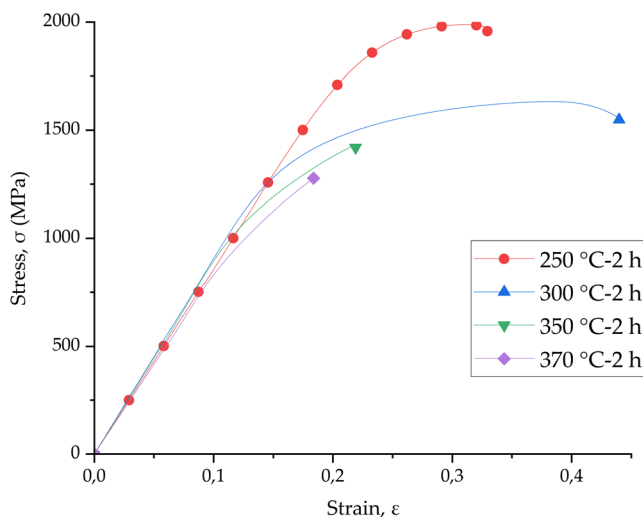
Figure 15. Engineering stress–strain curves of the specimens treated at different temperature.

premature fracture is probably related to two aspects: on the one hand, the incomplete transformation of austenite into bainitic ferrite leads to the presence of brittle martensite during final cooling derived that may deplete the mechanical response. On the other hand, at high temperatures the size of the blocks and films of retained austenite implies the strain-induced
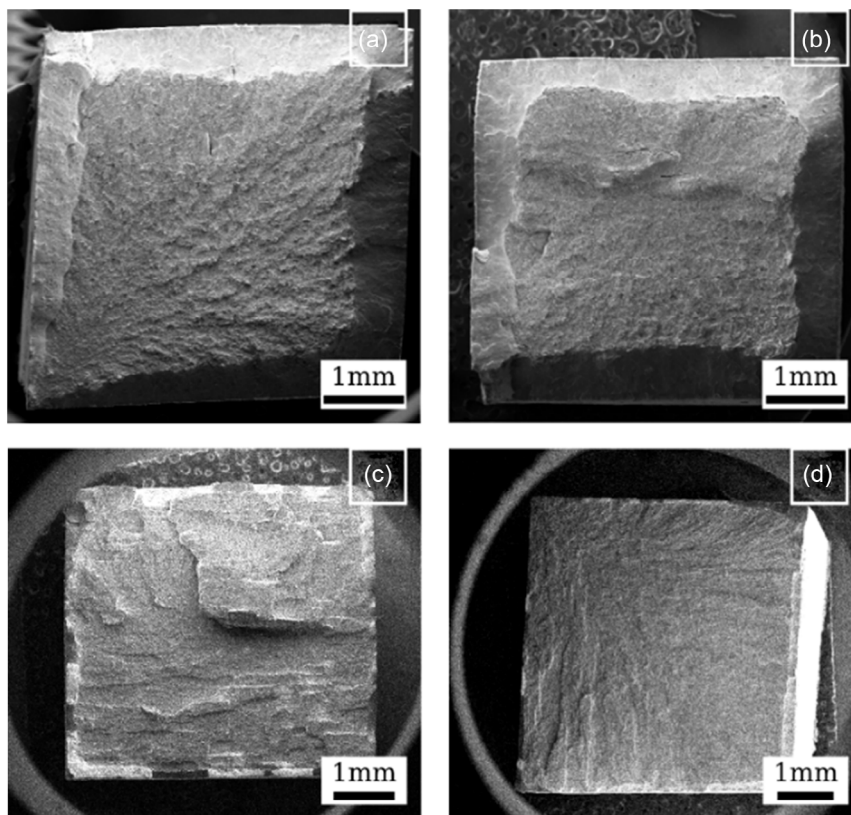
Figure 16. Low-magnification scanning electron micrographs of fracture surfaces for samples isothermally held for 2 h at: a) 250 °C, b) 300 °C, c) 350 °C, and d) 370 °C.

**ADVANCED
SCIENCE NEWS**

www.advancedsciencenews.com

**steel
research**
international

www.steel-research.de

Table 3. Results of the Rietveld refinement.

Austempering temperature [°C]	V_γ [vol%]	x_γ [wt%]	V_α [vol%]	x_α [wt%]
250	6 ± 3	1.22 ± 0.04	94 ± 3	0.18 ± 0.04
300	11 ± 3	1.01 ± 0.04	89 ± 3	0.13 ± 0.04
350	13 ± 3	0.82 ± 0.04	87 ± 3	0.15 ± 0.04
370	11 ± 3	0.71 ± 0.04	89 ± 3	0.16 ± 0.04

Table 4. Mechanical properties of CFB steel isothermally treated at different temperature above M_s.

| Austempering temperature	$\sigma_{0.2}$ [MPa]	σ_{UTS} [MPa]	Uniform elongation	ε_f
250	1638 ± 5	1988 ± 4	0.31 ± 0.01	0.33 ± 0.01
300	1150 ± 4	1632 ± 5	0.38 ± 0.01	0.44 ± 0.01
350	973 ± 5	1427 ± 5	0.22 ± 0.01	0.22 ± 0.01
370	886 ± 3	1276 ± 7	0.18 ± 0.02	0.18 ± 0.02

transformation phenomena at the early stage of the transformations[23] because the increase in energy required for crack propagation at high temperatures of bainite formation.[55] As argued by Zhao,[23] large blocks present at high temperatures, which low carbon enriched compared to the films, and contain a large number of nucleations site for martensitic transformation, tend to transform at low strain levels favouring the premature fracture. The driving force for the TRIP effect, in fact, is enlarged as the size of the blocks increases and the carbon content is reduced.

Thus, both are not able to sustain large elongations and suppress the cracks propagation that are forming at the interface between the different microstructural constituents.[56] Furthermore, the superior mechanical behavior both in terms of strength and elongation for the specimen treated at low temperatures should be ascribed to the thickness of the bainitic ferrite plates. As demonstrated by Garcia-Mateo et al.,[57] bainitic ferrite represent the strong phase with the CFB mictrostructure and provide a major contribute to the the high strength. Compared to retained austenite it is characterized by high capability accommodate high plastic deformations, acts as a barrier against the movement of the dislocations, and hinders cracks initiation and propagation.

Comparing the mechanical properties of this high-silicon bainitic steel with other results in the literature, it is evident that the performances are comparable to the ones of steels with similar microstructure and even superior, considering also the lower carbon content[8] (Table 4).

Low-magnification SEM fractographs of tensile test specimens are displayed in Figure 16. As evidenced by the micrographs, specimens isothermally held at 250 and 300 °C reveal a cup–cone appearance[58] confirming the ductile behavior shown also in the stress–strain curves, and the finer microstructure observed with SEM. On the other hand, specimens austempered at 350 and 370 °C exhibit a brittle fracture surface that does not show a reduction in the sample area, reflecting the behavior during mechanical testing and correlated with the presence in the microstructure of large martensitic islands.

The fracture surfaces of the tensile specimens were deeply observed with SEM (Figure 16) also at high magnification. The fracture surface of specimens treated at 250 °C and 300 °C was characterized by essentially ductile features with
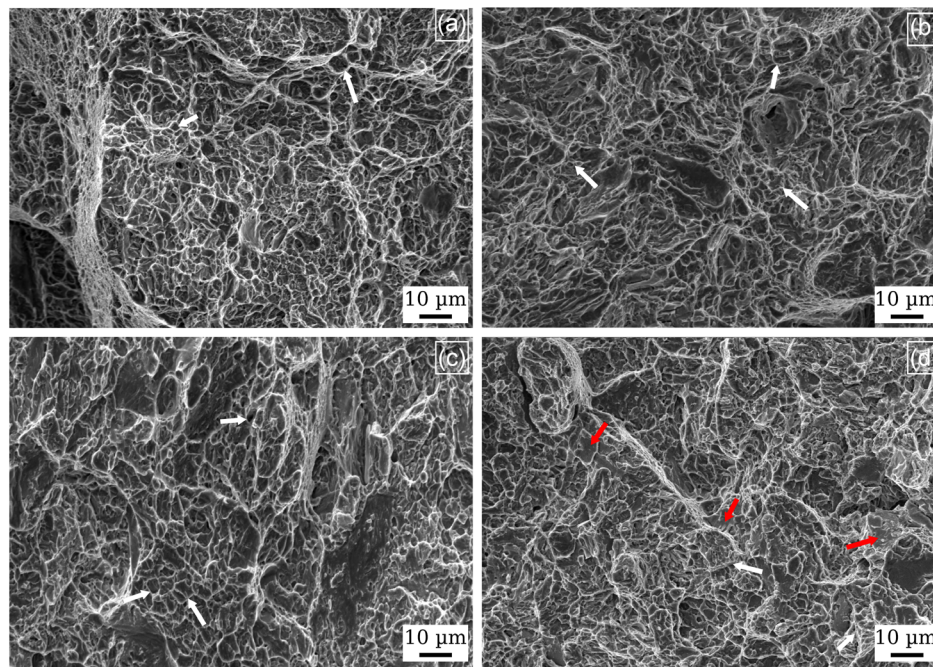
Figure 17. High-magnification scanning electron micrographs of fracture surfaces for samples isothermally held for 2 h at: a) 250 °C b) 300 °C, c) 350 °C, and d) 370 °C. White arrows indicate dimples; red arrows indicate quasicleavage facets.

2200821 (9 of 12)

Table 5. Amount of retained austenite after tensile test.

Austempering temperature	V_γ [vol%]	Reduction [%]
250	2 ± 3	67
300	3 ± 3	70
350	8 ± 3	38
370	6 ± 3	47

Table 6. Specimens Vickers microhardness and nanohardness before and after tensile stress.

Austempering temperature [°C]	$HV_{0.3}$ before tensile test	$HV_{0.3}$ after tensile test	Nanohardness [GPa] before tensile test	Nanohardness [GPa] before tensile test
250	509 ± 20	638 ± 30	6.9 ± 0.1	7.5 ± 0.6
300	487 ± 9	548 ± 32	5.6 ± 0.6	6.2 ± 0.5
350	455 ± 23	524 ± 33	5.2 ± 0.4	5.5 ± 0.4
370	491 ± 18	496 ± 34	6.0 ± 0.1	6.3 ± 0.6

the presence of dimples (white arrows in Figure 16a,b). In the samples treated at 350 and 370 °C also quasi-cleavage facets were present (red arrows in Figure 16c,d), indicating a brittle fracture component.

XRD tests were performed on the samples after the tensile tests (**Figure 17**) and the amount of retained austenite was calculated by Rietveld (**Table 5**). A significant reduction of retained austenite in all samples resulted in a comparison with the values reported in Table 2, and this was related to TRIP effect, i.e., transformation of retained austenite due to strain application.[15]

It should be noted that in the specimens treated at 370 and 350 °C, the peak of austenite is still present and the reduction of austenite was less marked. Considering that in these samples the retained austenite was mainly present in the form of large blocks, the lower values of both tensile and ductility can be

related to the transformation of the largest and with the lowest amount of carbon content into martensite at low strain values, confirming the previous results. The less marked reduction is suggesting again that the transformation of the blocks provokes the rupture, with the preexisting martensite without leading to the hardening and the transformation of the films located within the sheaves.

In order to better understand the behavior of the samples treated at 250 and 300 °C, which exhibit the highest performance in terms of tensile properties and ductility, the microstructure close to the fracture surface was investigated by SEM (**Figure 18** and **19**). The elongated and fractured bainitic sheaves
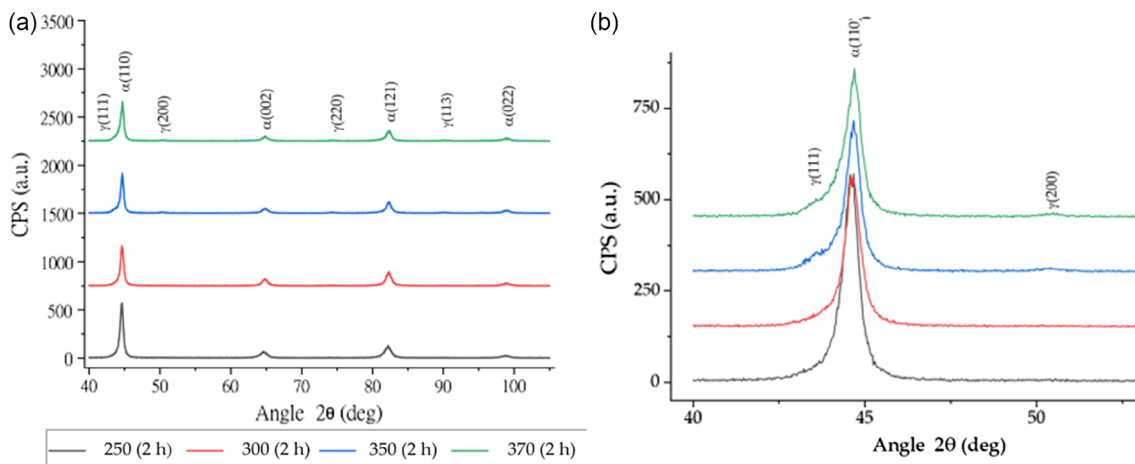
Figure 18. a) XRD patterns after tensile tests; b) zoom of the main austenite–ferrite peaks.
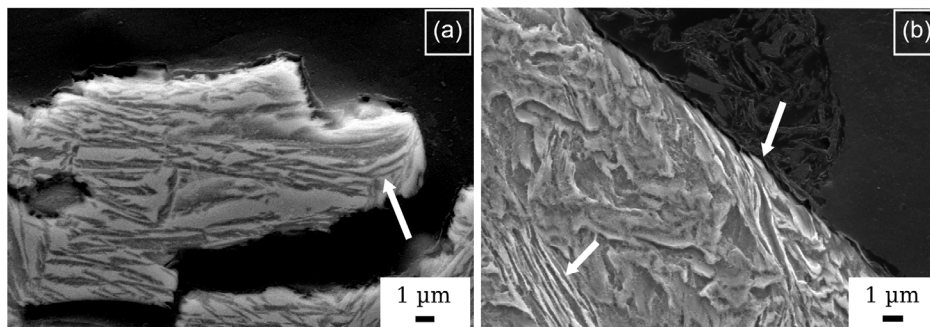
Figure 19. SEM image of specimen treated at a) 250 °C and b) 300 °C for 2 h after tensile test. White arrows in the figure indicate fractured and elongated retained austenite films.
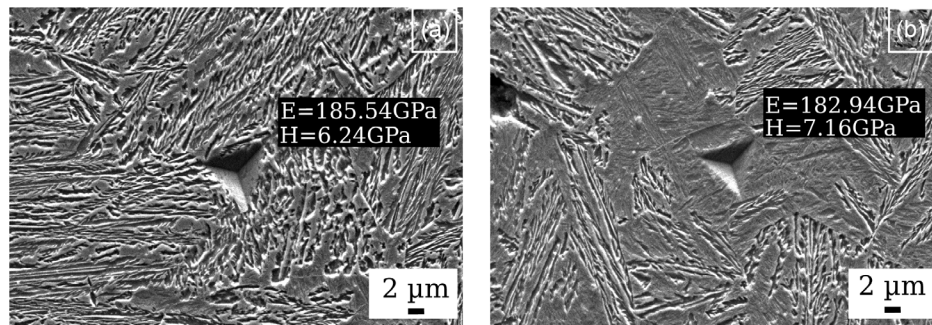
Figure 20. a,b) Nanoindentation performed on specimen austempered at 370 °C for 2 h.

observed in the samples demonstrate the high capability of bainitic ferrite to accommodate high-strain strains before failure, in agreement with Kumar.[59] Moreover, the presence of microcracks was only found at interfaces between bainitic sheaves and martensite blocks and not at austenite boundaries because thanks to the excellent plasticity of austenite, it is less probable that cracks initiate and propagate at the interface between austenite and the other phases.

3.6. Vickers Microhardness and Nanohardness

A progressive reduction in both micro- and nanohardness, increasing the isothermal holding temperature from 250 °C to 350 °C, due to the thicker plates of bainitic ferrite, was found in agreement with refs. [3,50] (**Table 6**). Additionally, a higher amount of brittle hard martensite, formed during the last cooling to room temperature, caused the hardness increase of the sample austempered at 370 °C. Performed measurements after tensile tests lead to observing an increase in hardness, partially due to strain-induced transformation phenomena (TRIP effect) of austenite in hard brittle martensite and the strain hardening induced during the tensile tests, accompanied by an increase in dislocation density.

In Figure 19, two nanoindentations are displayed on the different microstructural constituents. As expected, martensite (Figure 19b) exhibits higher hardness compared with carbide-free bainite (**Figure** 19a and **20**).

4. Conclusions

The effect of different austempering temperatures on a high-silicon CFB steel was studied. After microstructural investigation and mechanical tests, it is possible to conclude that: 1) Austempering above the martensite start temperature allowed to obtain a multiphase microstructure consisting in carbide-free bainite, with interplate filmy retained austenite, blocky retained austenite, and untempered martensite; 2) Increasing the austempering temperature produced a progressive coarsening of bainitic sheaves. At 250 °C it was possible to observe the lower amount of retained austenite at room temperature and as temperature increased, the amount of carbon in austenite decreased, in accordance with other results in literature. The retained austenite at 250 °C was preferentially with film like morphology,

whereas at higher temperature it assumed also a significative blocky one; 3) In general, the material exhibited excellent combinations of tensile strength and ductility, but it reached the highest strength values for the treatment at 250 °C with 33% of total elongation. This occurs, thanks to the nanostructured thickness of bainitic ferrite and the strain induced martensitic transfromation of the majority of the austenite, although the lowest amount of retained austenite in this sample, compared to those treated at higher temperatures. 4) Considering the combination of the mechanical properties, this newly developed steel represents a good alternative to pearlitic steel used nowadays in railway applications.

Conflict of Interest

The authors declare no conflict of interest.

Data Availability Statement

The data that support the findings of this study are available from the corresponding author upon reasonable request.

[1] J. Tian, G. Xu, Z. Jiang, X. Wan, H. Hu, Q. Yuan, *Steel Res. Int.* **2019**, *90*, 1800474.

[2] M. Franceschi, C. Soffritti, A. Fortini, L. Pezzato, G. L. Garagnani, M. Dabalà, *Tribol. Int.* **2023**, *178*.

[3] M. Franceschi, R. Bertolini, A. Fabrizi, M. Dabalà, L. Pezzato *Mater. Sci. Eng. A* **2023**.

www.steel-research.de

[4] M. Franceschi, A. Miotti Bettanini, L. Pezzato, M. Dabalà, P. J. Jacques, *Metals.* **2021**, *11*, 17.

[5] A. M. Gola, M. Ghadamgahi, S. W. Ooi, *Wear* **2017**, *376–377*, 975.

[6] C. Garcia-Mateo, F. G. Caballero, T. Sourmail, M. Kuntz, J. Cornide, V. Smanio, R. Elvira, *Mater. Sci. Eng. A* **2012**, *549*, 185.

[7] J. Y. Son, J. H. Kim, W. B. Kim, B. J. Ye, *Met. Mater. Int.* **2010**, *16*, 357.

[8] C. Garcia-Mateo, F. G. Caballero, *Handb. Mech. Nanostruct.* **2015**, *1*, 35.

[9] A. Kumar, S. K. Makineni, A. Dutta, C. Goulas, M. Steenbergen, R. H. Petrov, J. Sietsma, *Mater. Sci. Eng. A* **2019**, *759*, 210.

[10] V. G. Efremenko, O. Hesse, T. Friedrich, M. Kunert, M. N. Brykov, K. Shimizu, V. I. Zurnadzhy, P. Šuchmann, *Wear* **2019**, *418–419*, 24.

[11] S. P. Neog, S. D. Bakshi, S. Das, *Tribol. Int.* **2021**, *157*, 106846.

[12] F. G. Caballero, S. Allain, J. Cornide, J. D. Puerta Velásquez, C. Garcia-Mateo, M. K. Miller, *Mater. Des.* **2013**, *49*, 667.

[13] N. Krishna Murthy, G. D. Janaki Ram, B. S. Murty, G. M. Reddy, T. J. P. Rao *Mater. Trans. B. Process Metall. Mater. Process. Sci.* **2014**, *45*, 2327

[14] F. G. Caballero, H. K. D. H. Bhadeshia, K. J. A. Mawella, D. G. Jones, P. Brown *Mater. Sci. Technol.* **2002**, *18*, 279.

[15] N. Fonstein, in *Advanced High Strength Sheet Steels: Physical Metallurgy, Design, Processing, and Properties*, Springer, Cham **2015**.

[16] A. Kapito, R. J. Mostert, W. E. Stumpf, C. W. Siyasiya *IOP Conf. Ser. Mater. Sci. Eng.* **2019**, *655*, 012012.

[17] P. Valizadeh Moghaddam, J. Hardell, E. Vuorinen, B. Prakash, *Wear* **2020**, *454–455*, 203317.

[18] A. L. Bollinger, T. Murakami, K. O. Findley, E. De Moor, J. G. Speer, *Corrosion* **2019**, *75*, 888.

[19] Z. Changle, F. Hanguang, M. Shengqiang, L. Jian, L. Yongping *Mater. Res. Express* **2019**, *6*

[20] A. Barbacki, E. Mikołajski, *J. Mater. Process. Technol.* **1998**, *78*, 18.

[21] B. Fu, W. Y. Yang, L. F. Li, Z. Q. Sun, *Mater. Sci. Eng. A* **2014**, *603*, 134.

[22] H. Mousalou, S. Yazdani, B. Avishan, N. P. Ahmadi, A. Chabok, Y. Pei, *Mater. Sci. Eng. A* **2018**, *734*, 329.

[23] J. Zhao, B. Lv, F. Zhang, Z. Yang, L. Qian, C. Chen, X. Long, *Mater. Sci. Eng. A* **2019**, *742*, 179.

[24] T. Jiang, H. Liu, J. Sun, S. Guo, Y. Liu, *Mater. Sci. Eng. A* **2016**, *666*, 207.

[25] H. Mousalou, S. Yazdani, N. Parvini Ahmadi, B. Avishan, *Acta Metall. Sin.* **2020**, *33*, 1635.

[26] J. R. Yang, H. K. D. H. Bhadeshia *Phase Transform.* **1988**, *365–73*, 203.

[27] H. K. D. H. Bhadeshia, *Bainite in Steels: Theory and Practice*, Vol. 19, Maney Publishing, Leeds **2006**.

[28] M. Franceschi, L. Pezzato, A. G. Settimi, C. Gennari, M. Pigato, M. Polyakova, D. Konstantinov, K. Brunelli, M. Dabalà, *Materials* **2021**, *14*, 1

[29] M. Franceschi, L. Pezzato, C. Gennari, A. Fabrizi, M. Polyakova, D. Konstantinov, K. Brunelli, M. Dabalà, M. Dabal, *Metals* **2020**, *10*, 1448.

[30] X. Long, G. Zhao, F. Zhang, S. Xu, Z. Yang, G. Du, R. Branco, *Mater. Sci. Eng. A* **2020**, *775*, 138964.

[31] R. Kumar, R. K. Dwivedi, S. Ahmed, *Silicon* **2020**, *13*, 1249.

[32] P. A. Palaksha, K. S. Ravishankar *IOP Conf. Ser. Mater. Sci. Eng.* **2017**, *225*

[33] Z.Z. Zhao, H. X. Yin, A. M. Zhao, Z. Q. Gong, J. G. He, T.T. Tong, H. J. Hu, *Mater. Sci. Eng. A* **2014**, *613*, 8.

[34] Liu M., Xu G., Tian J. Y., Yuan Q, Chen X. *Int. J. Miner. Metall. Mater.* **2020**, *27*, 340.

[35] C. Garcia-Mateo, F. G. Caballero, J. Chao, C. Capdevila, C. Garcia De Andres, *J. Mater. Sci.* **2009**, *44*, 4617.

[36] J. P. Liu, Y. Q. Li, J. Y. Jin, Y. H. Zhang, F. S. Liu, R. Su, B. Narayanaswamy, Q. Y. Zhou *Mater. Today Commun.* **2020**, *25*.

[37] Z. Zhang, Li Y., Manabe K., Zhu F. *Mater. Trans.* **2012**, *53*, 833.

[38] K. Zhu, C. Mager, M. Huang, *J. Mater. Sci. Technol.* **2017**, *33*, 1475.

[39] L. Yuan, Q. Liu, H. Li, B. Gao, *Met. Sci. Heat Treat.* **2015**, *57*, 156.

[40] Tian J. Y., Xu G., Zhou M. X., Hu H. J., Xue Z. L. *J. Iron Steel Res. Int.* **2019**, *26*, 846.

[41] Stevens W., Haynes A. *J. Iron Steel Inst.* **1956**.

[42] C. Garcia-Mateo, J. A. Jimenez, B. Lopez-Ezquerra, R. Rementeria, L. Morales-Rivas, M. Kuntz, F. G. Caballero, *Mater. Charact.* **2016**, *122*, 83.

[43] L. Lutterotti, *Acta Crystallogr. A Found. Crystallogr.* **2000**, *56*, s54.

[44] C. B. Carter, D. B. Williams, *Trans. Electr. Microsc.* **1996**, 165.

[45] G. Gao, H. Zhang, Z. Tan, W. Liu, B. Bai, *Mater. Sci. Eng. A* **2013**, *559*, 165.

[46] A. Leiro, E. Vuorinen, K. G. Sundin, B. Prakash, T. Sourmail, V. Smanio, F. G. Caballero, C. Garcia-Mateo, R. Elvira, *Wear* **2013**, *298–299*, 42.

[47] L. Morales-Rivas, A. González-Orive, C. Garcia-Mateo, A. Hernández-Creus, F. G. Caballero, L. Vázquez, *Sci. Rep.* **2015**, *5*, article no. 17164.

[48] F. Y. Zhao, P. Chen, B. Y. Xu, Q. Yu, G. D. Wang, H. L. Yi, *Mater. Sci. Technol.* **2020**, *36*, 1704.

[49] H. K. D. H. Bhadeshia *Mater. Sci. Forum* **2005**, *500–501*, 63.

[50] A. Eres-Castellanos, L. Morales-Rivas, A. Latz, F. G. Caballero, C. Garcia-Mateo, *Mater. Charact.* **2018**, *145*, 371.

[51] X. Long, R. Zhang, F. Zhang, G. Du, X. Zhao, *Mater. Sci. Eng. A* **2019**, *760*, 158.

[52] S. Khare, K. Lee, H. K. D. H. Bhadeshia *Mater. Trans. A. Phys. Metall. Mater. Sci.* **2010**, *41*, 922.

[53] S. K. Putatunda, *Mater. Des.* **2003**, *24*, 435.

[54] C. Garcia-Mateo, J. A. Jimenez, H. W. Yen, M. K. Miller, L. Morales-Rivas, M. Kuntz, S. P. Ringer, J. R. Yang, F. G. Caballero, *Acta Mater.* **2015**, *91*, 162.

[55] N. Fonstein, H. J. Jun, G. Huang, S. Sriram, B. Yan, *Mater. Sci. Technol. Conf. Exhib. 2011, MS T'11* **2011**, *1*, 634.

[56] J. Zhao, F. Zhang, B. Lv, Z. Yang, C. Chen, X. Long, X. Zhao, C. Chu, *Mater. Sci. Eng. A* **2019**, *751*, 80.

[57] C. Garcia-Mateo, T. Sourmail, F. G. Caballero, V. Smanio, M. Kuntz, C. Ziegler, A. Leiro, E. Vuorinen, R. Elvira, T. Teeri, *Mater. Sci. Technol.* **2014**, *30*, 1071.

[58] H. Liu, S. Hamada, H. Noguchi, *IOP Conf. Ser. Mater. Sci. Eng.* **2020**, *774*.

[59] A. Kumar, A. Dutta, S. K. Makineni, M. Herbig, R. H. Petrov, J. Sietsma, *Mater. Sci. Eng. A* **2019**, *757*, 107.